ELECTROMAGNETIC COUPLING TO A WEARABLE APPLICATION BASED ON COAXIAL CABLE ARCHITECTURE

M. Chedid

Saab Training Systems AB
Stensholmsvägen 20, SE 56185, Huskvarna, Sweden

I. Belov

School of Engineering
Jönköping University
P.O. Box 1026, SE 55111, Jönköping, Sweden

P. Leisner

Acreo AB/School of Engineering
Jönköping University
P.O. Box 1026, SE 55111, Jönköping, Sweden

Abstract—A radiated susceptibility problem has been identified and solved by means of simulations for a wearable computer system in the frequency range 30 MHz–1 GHz. Simulation strategy is presented for analyzing the effects induced by an electromagnetic plane wave within the system comprising infra-red sensors connected by coaxial cables. A procedure of creating a TLM model of the coaxial cable with controlled electromagnetic coupling characteristics on a coarse grid is proposed. Results are verified by means of theoretical calculations. Different sensor enclosures and filtering circuits are analyzed and implemented to meet the hard electromagnetic compatibility requirements while not interfering with the functionality of the wearable application.

1. INTRODUCTION

In today's military domain, wearable computers are becoming an essential part of the soldier's equipment. Wearable computer is a system which includes sensors and communication modules located on different parts of the human body connected to a personnel computer unit (PCU) (see Fig. 1). The PCU measures and processes signals received from sensors and communication modules. Creating design solutions robust to external electromagnetic (EM) fields is of major concern for engineers in order to meet tough requirements of military specifications [1].
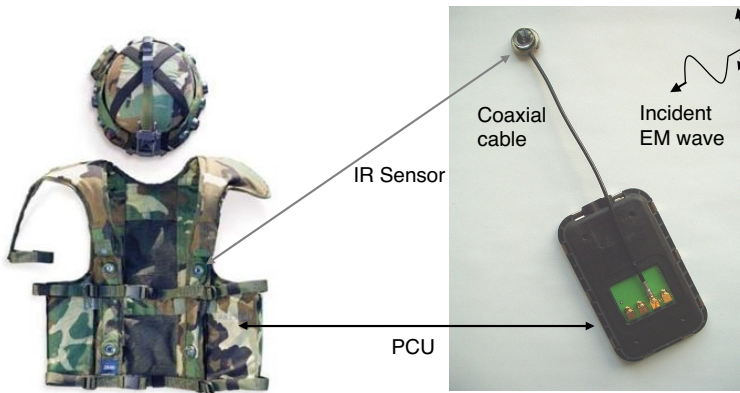

Figure 1. Studied wearable system.

This paper is focused on EMC modelling of a specific application used in a force-on-force military training system. The application consisted of a number of infra-red (IR) sensors, enclosed in metal boxes, distributed on the human body and connected to a PCU via coaxial cables. Sensors deliver analog signals with low amplitudes that need to be transported over a typical distance of 0.5 m–1 m. Due to cost reasons and assembly requirements, the shield of the coaxial cable cannot be peripherally bonded to the sensor box making the wearable system susceptible to external EM waves. The absence of low-impedance path to a ground plane (GP) makes the task of shielding the wearable system even more difficult. EMC tests revealed radiated susceptibility of the wearable system. However, the cause of the problem and efficiency of possible engineering solutions had to be studied carefully. Therefore, an EMC modelling strategy was proposed, including a procedure for creating a Transmission Line Matrix (TLM) model of a coaxial cable with controlled EM coupling characteristics.

The study starts with a case description where specification of the system is provided and the EMC problem is indicated. The EMC modelling strategy is then presented including comparison between different models of a coaxial transmission line (TL) [2, 3]. Furthermore, verification of simulation results to theoretical calculations of EM coupling was done [4–6]. The EM coupling problem was demonstrated, and solved by means of simulations. The quality of the obtained results was confirmed by EMC testing of the fully assembled wearable computer application. Finally, conclusions were formulated to address EM coupling problems in wearable systems.

2. CASE DESCRIPTION

The studied application included a photodiode inside a metal box, a low noise coaxial cable having the length 50 cm and a transimpedance amplifier inside a shielded PCU. The choice of coaxial cable was based mainly on mechanical requirements. The cable should be flexible to withstand bending, fluctuations of pressure, friction and torsion. The cross-sectional dimensions and electrical properties of the cable are listed in Table 1. The semi-conductive layer, between the dielectric and shield layers, reduces electrical noise induced by mechanical stress on the cable.

Table 1. Coaxial cable data.

Layer	Outer diameter (mm)	Material
Inner conductor	0.4	Copper
Dielectric	1.4	Solid polyethylene
Semi-conductive layer	1.9	PVC and graphite
Shield	2.40	Silver coated copper
Jacket	3.15	PVC

The main function of the application is to detect a message represented by a sequence of low intensity IR pulses. The information in the message is encoded by means of distances between the pulses. A high degree of accuracy and resolution is required in order to decode the message correctly. The incident IR light allows a current ($0.5\,\mu A$–$1\,\mu A$) to flow through the photodiode which is fed into the transimpedance amplifier. The result is a voltage that is a linear function of the applied light intensity which can be detected for further processing (see Fig. 2). The bandwidth of the amplifier is 10 MHz with a trans-resistance of $0.3\,M\Omega$.
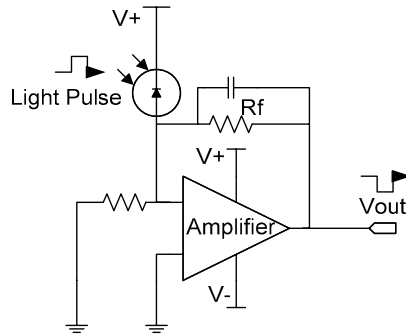
Figure 2. Principle schematic of the detection function in the wearable system.

At the PCU, the coaxial cable is connected through a COTS coaxial connector while at the sensor box a custom designed connection is made in order to meet size and assembly requirements. The basic design of the sensor box has a circular shape with two concentric metal cylinders (see Fig. 3). The outer cylinder has a diameter of 24 mm and the inner cylinder has a diameter of 14 mm. The photodiode is soldered in the inner cylinder while the cable shield is soldered between the outer and inner cylinder. The latter was done with the intention to improve shielding effectiveness while being able to use the cable shield as a return path for the current. The top of the sensor is then encapsulated with a metal cover having small apertures to let the IR light get to the photodiode.
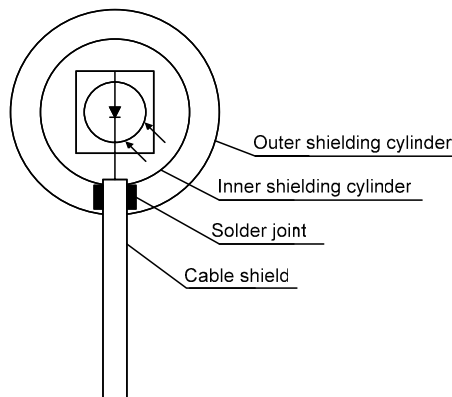

Figure 3. Top view of the sensor box.

Immunity of the system to $50\,\mathrm{V/m}$ EMI was tested according to the standard MIL-STD-461E RS103 [1] for the frequency range $30\,\mathrm{MHz}$–$1\,\mathrm{GHz}$. The tests and circuit analysis showed that if the current at the amplifier input exceeded $560\,\mathrm{nA}$ limit, i.e., $-125\,\mathrm{dB}$ (in the following $0\,\mathrm{dB}$ corresponds to $1\,\mathrm{A}$), with adequate spectral content then it would be amplified and interpreted as an IR pulse resulting in false detection alarms. A possible explanation is that the incident EM wave induces current on the external surface of the cable shield which is then coupled to the inner conductor and thus resulting in a noise current at the transimpedance amplifier. Although the frequency of the incident wave is much higher than the bandwidth of the amplifier, the induced current is demodulated at the amplifier input and consequently amplified. The following EMC modelling strategy investigates EM coupling paths and introduces methods to improve signal to noise ratio in the system.

3. EMC MODELLING STRATEGY

Simplifications are very common when building simulation models in order to shorten the computational time. However the applied simplifications should not jeopardize the integrity of the results, taking into account fundamental physical phenomena. Fig. 4 presents the flowchart of the EMC modelling strategy that consists of three main steps. First, a model of the coaxial TL was constructed where the major part was dedicated to verification purposes. The main goal
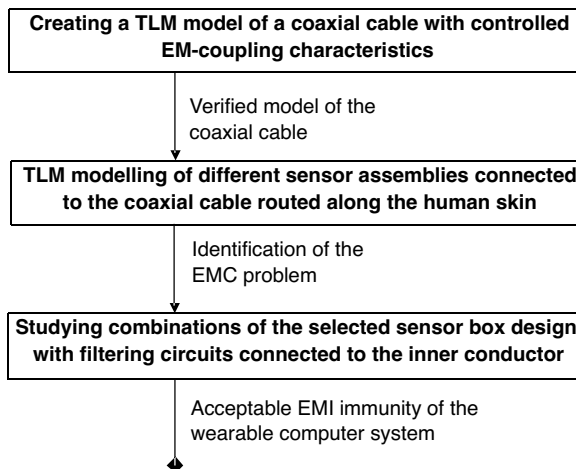

Figure 4. EMC modelling strategy for the wearable system.

was to guarantee that the simulated coupling paths and modes can be explained and predicted analytically based on cable dimensions. Secondly, the EM-coupling to the wearable system was studied in order to identify the EMC problem. Different geometries of the sensor assembly were evaluated and compared in this step. Last, electrical filtering circuits were designed and introduced to complement the mechanical measures from previous step to further reduce the noise current induced on the inner conductor.

A 3D electromagnetic field simulation program, FloEMC from Flomerics, was chosen for EMC modelling of the wearable system. This tool employs the TLM method to solve Maxwell's equations in time domain. The frequency domain information is then extracted by using FFT technique. The computational mesh consisted of cuboids of different sizes with an option of cell combining. Coaxial cable elements were modelled by solid blocks and the sensor box walls were approximated by thin plates with holes for cable entry. The TLM model was excited by $1\,\mathrm{V/m}$ plane wave propagating in the direction normal to the cover of the sensor box, with E-field vector directed along the cable. Absorbing boundary conditions were used to represent open faces of the computational domain. Convergence tests were undertaken to determine the effect of the open boundary location on the simulation results. Convergence criterion was satisfied when initial system energy decayed by at least $60\,\mathrm{dB}$.

4. IMPLEMENTATION AND RESULTS

The implementation begins with building models of the electronic circuits of the sensor and the transimpedance amplifier. Fundamentally, a photodiode is a current source when illuminated. When not conducting the photodiode can be approximated by a shunt resistor and a junction capacitance connected in parallel [7]. The value of the shunt resistance is usually high (several $\mathrm{M}\Omega$) and was therefore neglected. The junction capacitance of the photodiode depends both on the junction area and on the bias voltage. From data sheets, the junction capacitance was approximated to $22\,\mathrm{pF}$ at a bias voltage of $5\,\mathrm{V}$. The transimpedance amplifier was seen as "black box" and was replaced by its small signal input impedance. Using PSpice simulations, it was approximated to $20\,\Omega$ in the frequency range of interest $30\,\mathrm{MHz}$–$1\,\mathrm{GHz}$ (see Fig. 5).

4.1. TLM Model of a Coaxial Transmission Line

The introduced models of the electrical circuits were connected together with a coaxial cable. In order to create a TLM model of
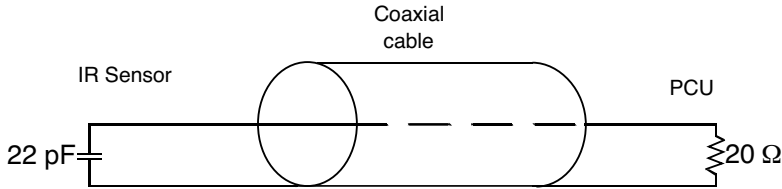
Coaxial
cable

IR Sensor   PCU

22 pF   20 Ω

Figure 5. Schematic of the coaxial transmission line.

PROCEDURE FOR CREATING A TLM MODEL OF A COAXIAL CABLE WITH CONTROLLED
EM-COUPLING CHARACTERISTICS

1 Selecting a method of modelling a
square cross-section coax cable with given Zo

S-parameter TLM modelling, coaxial line with ε_r:
- Circular cross-section cable, semi-infinite
- Method A, semi-infinite
- Method B, semi-infinite
- Method B-modified, semi-infinite
- Method B-modified, finite length L

2 Modelling EM-field coupling to the coax cable
shield

Far field coupling to a cylindrical wire above a
perfect conducting GP:
- TLM, Thin-wire model of cable shield
- MoM, cylindrical wire
- Analytical solution, integral equation for wire
antenna

Far field coupling to a square-cross-section wire
above a perfect conducting GP:
- TLM, solid model of cable shield, L
- TLM, modified length of cable shield, L'

3 Compensating the cable internal electrical and
geometrical properties

S-parameter TLM modelling, coax. line with ε_r':
- Method B-modified, finite length L'

4 Verifying the EM-coupling modes through the
imperfect shield for the selected model

Far field coupling to coaxial cable above a perfect
conducting GP:
- TLM, multiple slots on the sqaure cross-section
cable shield
- Analytic solution of TL equations for circular cross-
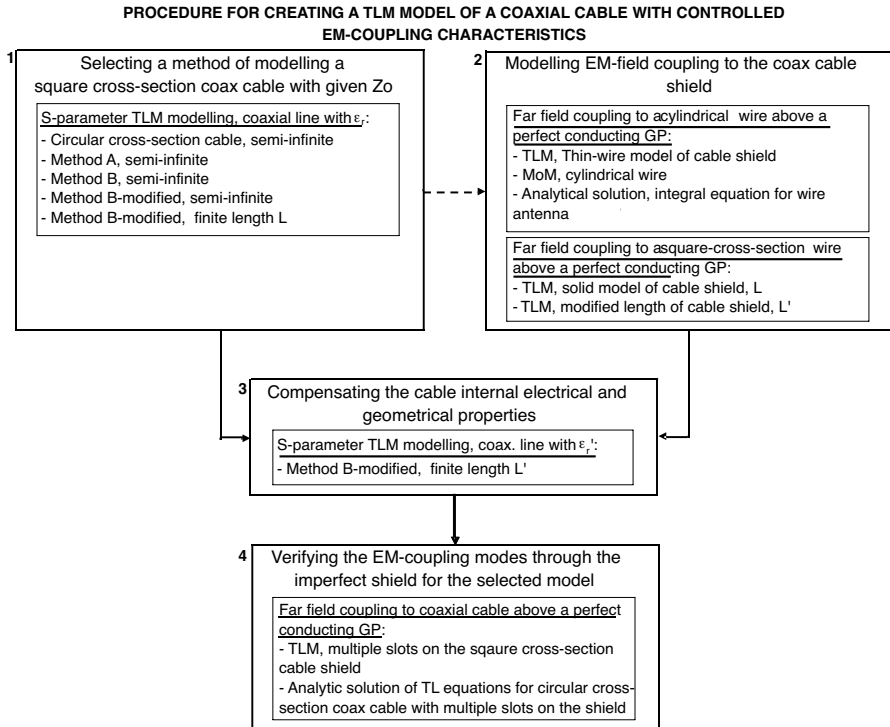section coax cable with multiple slots on the shield

Figure 6. Procedure for building a coaxial cable model.

the cable with controlled EM-coupling characteristics, the following
procedure was introduced (see Fig. 6).

*Selecting a method of modelling square cross-section coax cable
with given characteristic impedance Z_0.* The semi-conductive layer
in the cable was neglected since mechanical issues were out of scope
of this paper. Semi-conductive layer is of such resistance that when
applied between the shield and dielectric of the coaxial cable, the
adjacent surfaces of these two layers will maintain substantially the

same potential. Extending the internal surface of the shield layer towards the dielectric layer would thus not be of much significance for the electrical transmission properties of the line.

The cable with the data presented in Table 1 has a circular shape. Rectangular geometries are more suitable to use when building the model reducing the number of cells in the computational domain. Therefore a square cross-section of the cable was adapted (see Fig. 7), having same capacitance per unit length properties and consequently same $Z_0 = 50\,\Omega$. Two transformation methods were studied and compared for the TLM model of the semi-infinite cable: the first method (Method A) was introduced in [2] and the second method (Method B) was known from [3].
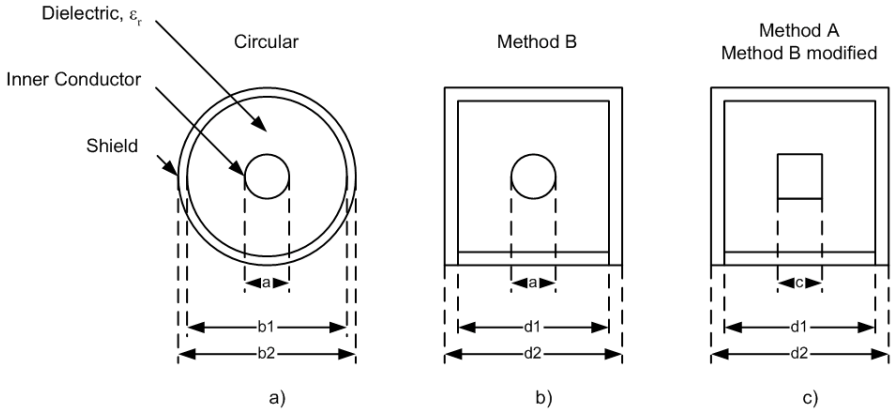
Figure 7. Comparison of cross-section geometries for different methods.

In Method A, using the variational extreme value theory, the characteristic impedance of a square coaxial cable was computed by (1):

$$Z_0 = \frac{1}{8 \tan\left(\dfrac{\pi}{4}\right)} \ln\left(\frac{d_1}{c}\right) \sqrt{\frac{\mu_0}{\varepsilon_r \varepsilon_0}}, \tag{1}$$

where d_1 is the inner side length of the square shield and c is the side length of the inner conductor (see Fig. 7c). In Method B, (2) was supplied to compute the characteristic impedance of a coaxial line with a square shield and a circular inner conductor with diameter a (see Fig. 7b):

$$Z_0 = \frac{60}{\sqrt{\varepsilon_r}} \ln\left(1.08\frac{d_1}{a}\right). \tag{2}$$
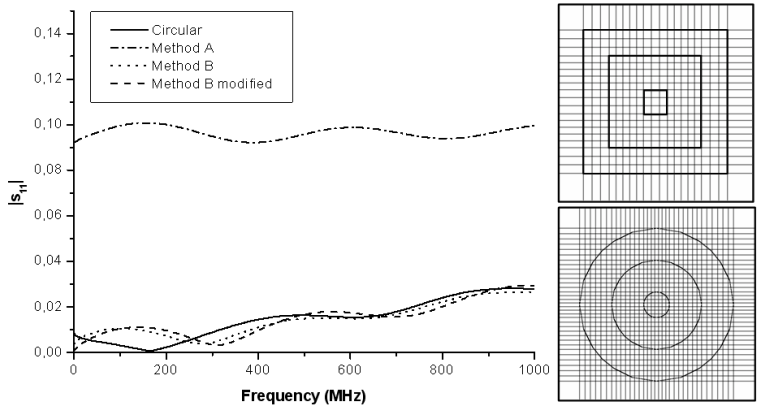
Figure 8. Spectrum of s_{11} for different coaxial cable models (left) and grid densities for circular and square cross-sections (right).

The equivalent side length of a square cross-section conductor, s, which has the same self impedance as a circular cross-section conductor with diameter D, can be calculated by (3) [8]:

$$s = \frac{D}{1.18}. \tag{3}$$

Model B was modified to include a square inner conductor by combining (2) and (3). Table 2 summarizes the dimensions of the different layers in the square coaxial cable using methods A, B and B-modified.

Table 2. Cross-sectional dimensions of different coaxial cable models.

	Circular	Method A	Method B	Method B-modified
Inner conductor (mm)	$a = 0.40$	$c = 0.34$	$a = 0.40$	$c = 0.34$
Dielectric (mm)	$b_1 = 1.4$	$d_1 = 1.68$	$d_1 = 1.31$	$d_1 = 1.31$
Shield (mm)	$b_2 = 3.15$	$d_2 = 2.03$	$d_2 = 2.03$	$d_2 = 2.03$

Having calculated the dimensions of the cable, TLM simulations were done in order to make model selection for further study. The circular model has to be densely meshed in order to capture the geometrical features of the cross-section whereas the square cross-section model can be built on a coarse mesh. One-port scattering parameters simulations with semi-infinite length were done. The port

impedance was set to $50\,\Omega$. The results are shown in Fig. 8. Both method B and B-modified delivered similar results. The magnitude of s_{11} had a maximum value of 0.03 meaning that very small reflection occurs at the port. Consequently the TL had the same impedance as the port impedance. The results of Method A show that the impedance of the TL was different from the port impedance. Method B-modified was found more suitable for TLM modelling and therefore chosen.

Modelling EM-field coupling to the coax cable shield. In the previous section, the cross-sectional properties of the coaxial cable were considered. However the incoming EM-wave couples to the external shield where the total length of the cable plays the major roll in determining the coupling modes. An extensive study was done to assure an exterior response of the model that corresponds to the theoretically predicted results. This study was based on a simple wire model having the same cross-sectional dimension of the cable shield. The inner layers were not included. The wire was placed 1 cm above a perfectly conducting GP. The verification includes four different coupling models:

- Model 1: Approximate theoretical model using a simplified solution of the integral equation for wire antenna current.
- Model 2: MoM model of a wire antenna.
- Model 3: TLM model of a thin wire antenna.
- Model 4: TLM model of a square cross-section wire.

The induced current in the middle of the wire was monitored in all models and compared to each other. In [4], the current induced on a wire antenna by a far field plane wave with an electric field magnitude, E_0, is approximately given by (4):

$$I_s(z) = j\frac{4\pi E_0}{Z_0 \Omega_0 k}\left(\cos(kz) - 1 + (1 - \cos(kL))\frac{\sin(kz)}{\sin(kL)}\right), \quad (4)$$

where z is the coordinate along the wire, $\Omega_0 = 2\ln(L/a)$, $L = 50\,\text{cm}$ is the total length of the wire, $a = 0.20\,\text{mm}$ is the radius of the wire, $Z_0 = 377\,\Omega$ is the free space wave impedance, $k = 2\pi f/c$ is the wave constant, f is the frequency and c is the speed of light in free space.

The resulting magnitudes of current from models 1–3 are plotted in Fig. 9. A good agreement between the models concerning the location of the resonant frequencies when the total length $L = \lambda/2, 3\lambda/2$, and so on, was observed. The approximate analytical solution suffers from poles at the resonant frequencies where the current is infinite. This is not seen in the figure due to the fact that the sampling points do not coincide with the resonant frequencies.
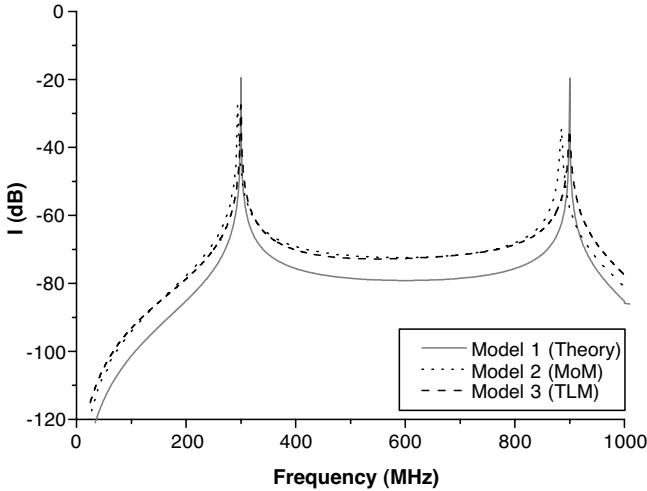
Figure 9. Induced current spectrum in the middle of thin wire antenna.

The current in the middle of the wire in model 4 was not possible to observe, and therefore the induced H-field was monitored instead, in the vicinity of the middle of the solid. Fig. 10 shows the magnitude of the H-field for model 4 and model 3. The solid model showed lower resonant frequencies than expected due to the poor pulse communication which is typical problem for TLM-based methods [9]. A possible solution would be to increase the resolution of the grid surrounding the wire structure, hereby increasing simulation time to unreasonable limit compared to the simplicity of the solid conductor model considered here. A rather straightforward idea is to shorten the length of the cable and consequently increasing the resonant frequencies. By examining the previous results, it was estimated that a shortening of 2 cm would furnish the desired results (see Fig. 10). The resonant frequencies for the solid with modified length were found more consistent with results from the thin wire TLM model.

Compensating the cable internal electrical and geometrical properties. A shorter cable requires adjustments of the internal properties in order to have the same signal propagation time as for the original longer model. Requesting the same propagation time between the ends of the cables leads to (5).

$$\frac{L}{v} = \frac{L'}{v'} \Leftrightarrow L\sqrt{\varepsilon_r} = L'\sqrt{\varepsilon_r'} \tag{5}$$
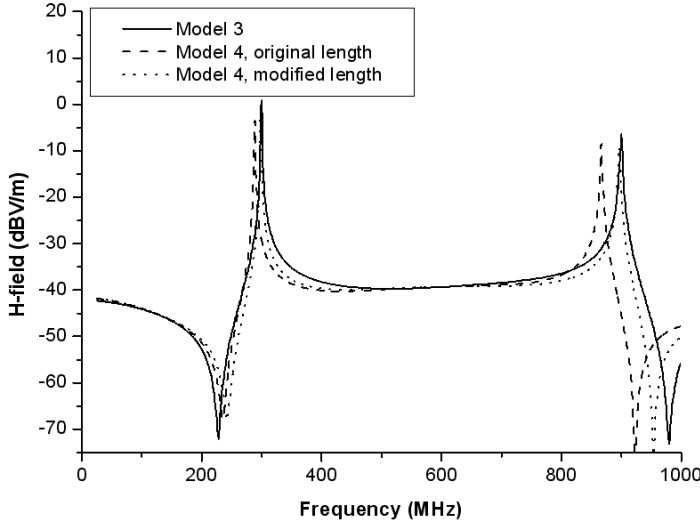
Figure 10. Spectrum of the induced H-field around the wire approximated by the solid cuboid and the thin wire TLM model.

where L and L' are the original and modified lengths, respectively, v and v' are the wave propagation velocities corresponding to original and modified relative permittivities ε_r and ε_r', respectively. Changing permittivity would consequently alter the characteristic impedance of the cable computed in step 1. Redoing the calculations, according to method B-modified selected in step 1, with the new value of relative permittivity, $\varepsilon_r' = 2.45$, gives new crossectional dimensions of the cable with the required characteristic impedance, $50\,\Omega$. Table 3 summarizes the final dimensions of the modified cable.

Table 3. Final data for the TLM model of the square coaxial cable.

Inner conductor, c	Dielectric, d_1	Shield, d_2	Length, L'	Relative permittivity, ε_r'
0.34 mm	1.35 mm	2.03 mm	48 cm	2.45

Fig. 11 shows characteristics of the modified cable compared to the original cable ($\varepsilon_r = 2.3$, $L = 50\,\text{cm}$), both modelled according to the B-modified method. The simulations were performed on cables having finite lengths. The magnitude of s_{11} was mainly the same for both cables. An additional simulation was performed on the modified cable with another TLM program, Microstripes from Flomerics, where
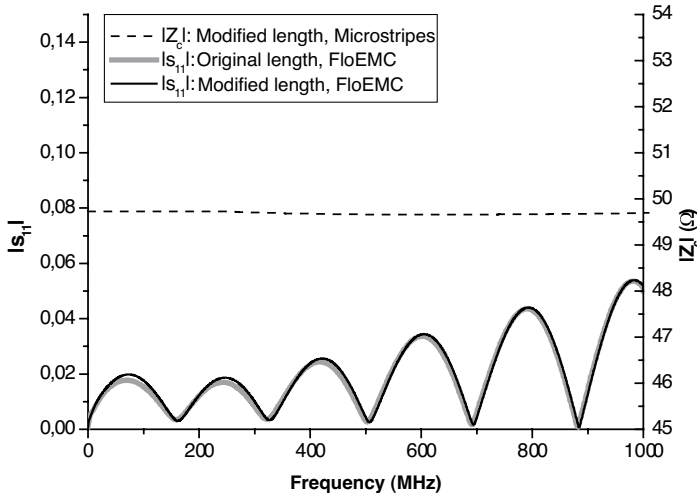
Figure 11. Magnitude of s_{11} of the original and modified cable and Z_c of the modified cable.

the characteristic impedance can be monitored directly. The model of the modified cable provides a characteristic impedance of $49.7\,\Omega$, thus confirming the choice of the cable internal properties in the TLM model.

Verifying the EM coupling modes through the imperfect shield. Coupling to coaxial cables has been studied in different publications [5, 6]. The coaxial TL is usually represented as a system that consists of two transmission lines, external and internal. The voltage and current, induced by the incident EM field on the external TL, induce in their turn voltage and current on the internal TL due to existing apertures on the cable shield where leakage of the external incident EM field occurs. In the case studied here, it was not possible to model the exterior of the shield as a TL with ground as return path due to isolation of the TL from the GP. Assuming that the cable is located $1\,\mathrm{cm}$ above the perfectly conducting GP, (4) gives the common mode external current induced on the cable shield. Knowing the induced current and the shunt admittance per unit length Y between the cable shield and the GP, the induced voltage V_s can then be calculated according to (6):

$$V_s(z) = -j\frac{4\pi E_0}{Y Z_0 \Omega_0}\left(\sin(kz) - 1 + (1 - \cos(kL))\frac{\cos(kz)}{\sin(kL)}\right), \qquad (6)$$

Given the external shield current and voltage, I_s and V_s, calculated using (4) and (6) respectively, the internal current and voltage, I_i and V_i, are described by (7) [4]:

$$\begin{cases} \dfrac{dV_i}{dz} + jwl'(1+\Delta_l)I_i = Z_tI_s \\ \dfrac{dI_i}{dz} + jwc'(1-\Delta_c)V_i = -Y_tV_s \end{cases}, \tag{7}$$

where $\Delta_l = l_a/l'$, $\Delta_c = c_a/c'$, l' and c' are the per unit length inductance and capacitance of the inner part of the coaxial cable, respectively; l_a and c_a are the effective apertures inductance and the effective aperture capacitance, respectively, and Z_t and Y_t are the transfer impedance and transfer admittance of the cable shield, respectively.

Using a commercially available computational tool, Maple, the spectral content of the internal voltage and current was calculated from (7) for the cable loaded by 22 pF capacitor on the sensor end, and by 20 Ω resistor on the PCU end. A number of apertures uniformly distributed were introduced on the shield of the modified cable model. The apertures were modelled as slits with a width of 0.13 mm, a length of 1.3 mm and a pitch of 5 mm (see Fig. 12).
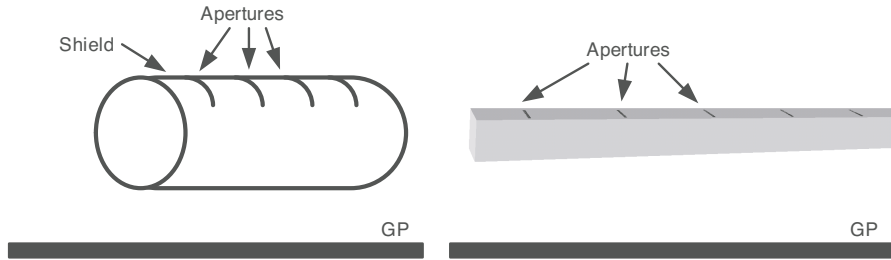

Figure 12. Cable shield with apertures above GP: theoretical model (left) and TLM model (right).

In Fig. 13, both theoretically predicted internal current spectrum at the PCU end is plotted as well as that provided by TLM solver. Increase in the number of resonant frequencies was noticed compared to the EM coupling to external shield (300 MHz and 900 MHz). The other resonances appeared due to the internal TL where impedance mismatch was the main contributor and their locations were dictated by the internal properties of the cable. For example, the resonances at 400 MHz and 800 MHz correspond to $L' = \lambda$ and 2λ, respectively, taking into account $\varepsilon'_r = 2.45$. While the location of resonances is
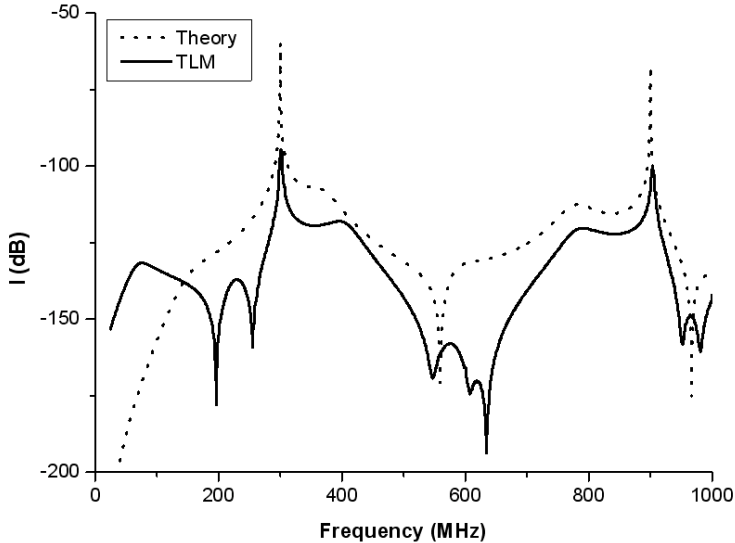
Figure 13. Comparison of current spectrum between theoretical and TLM models for the coaxial cable with uniformly distributed slits, above a perfectly conducting GP.

similar in both models, the level of the induced current was generally higher when considering the theoretical model. This is due mainly to the fact that in the TLM model the slits had the depth equal to the thickness of the cable shield, which reduced coupling efficiency. In the theoretical model the slits were modelled as infinitely thin.

4.2. TLM Modelling of the Sensor Assembly

In the previous sections the model of the coaxial cable was introduced and analytically verified. As mentioned before, the sensor was attached to the coaxial cable by a custom made connection. This connection was thought to be the weakest point of the system and therefore of high importance to study. The model was built by replacing the circular shaped sensor box by rectangular shaped box with two concentric enclosures (see Fig. 14). In order to have a better view of the sensor box construction, the top cover was removed in the figure. The small apertures on the top cover were neglected in the simulations due to their small electrical dimensions at the highest frequency of interest.

In order to evaluate the effect of different sensor box geometries on the EMC performance, three cases were considered (see Fig. 14):
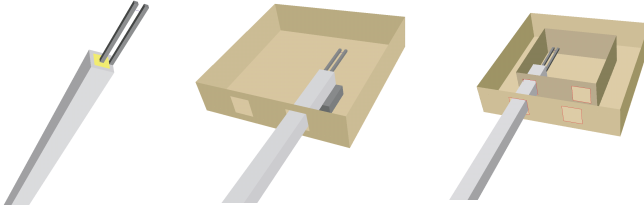
Figure 14. TLM model of the wearable system without sensor box (left), single shielded sensor box (middle) and double shielded sensor box (right).

1. No sensor box.
2. Sensor box with single shield.
3. Sensor box with double shield.

Furthermore, the perfectly conducting GP was replaced by a layer representing the human skin to have a more consistent model with the real user environment. Although the electrical properties of the skin vary with frequency, these remain relatively stable between 100 MHz and 1 GHz [10]. Therefore, the permittivity and conductivity of the skin at mid-frequency (500 MHz) were chosen for simulation $\varepsilon_r = 40$, $\sigma = 0.45$ S/m). The current at the amplifier end was monitored and shown in Fig. 15 for each of the three cases. The introduction of the lossy dielectric (skin) altered obviously the location of the resonances. The straight line in Fig. 15 indicates the maximum level of current -165 dB allowed at the amplifier input when the incident E-field strength is 1 V/m. This level was derived by normalizing the lowest acceptable noise current mentioned before (560 nA) to the E-field strength 50 V/m. The limit was further lowered by 6 dB in order to have sufficient performance margin. The high shielding effectiveness of the metal box is clearly seen in Fig. 15. The double shielded sensor box showed an average of 10 dB higher shielding effectiveness than single shielded box and was therefore chosen. Two critical regions were identified: one between 200 MHz and 300 MHz and one between 700 MHz and 1 GHz. A reduction of approximately 20 dB is required to obtain a satisfactory EMC design.

4.3. Combination of the Sensor Box Design with EMI Filtering Circuits

EMI filtering circuits are considered in this section as a complementary EMC design measure. The main function of these circuits is to attenuate undesired frequency components and to prevent noise
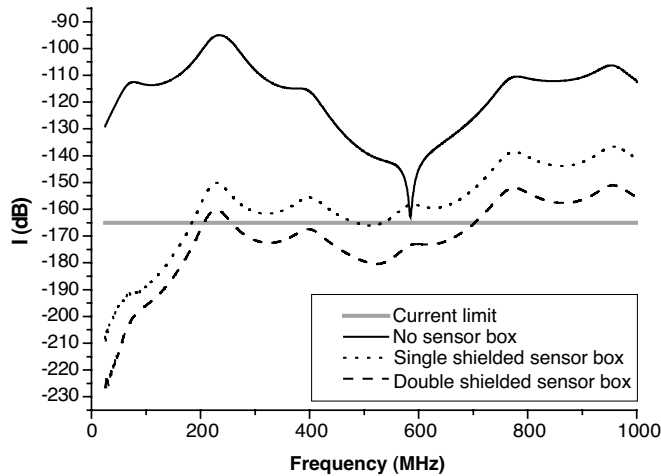
Figure 15. Current spectrum at the PCU end for different sensor box geometries.

currents from reaching sensitive parts of the design. However, impedance matching is in many cases not included in commercially available filter circuits. In order to reduce the noise current reflection, an impedance matching network was then introduced to the EMI filter. The structure of the studied filter is presented in Fig. 16.
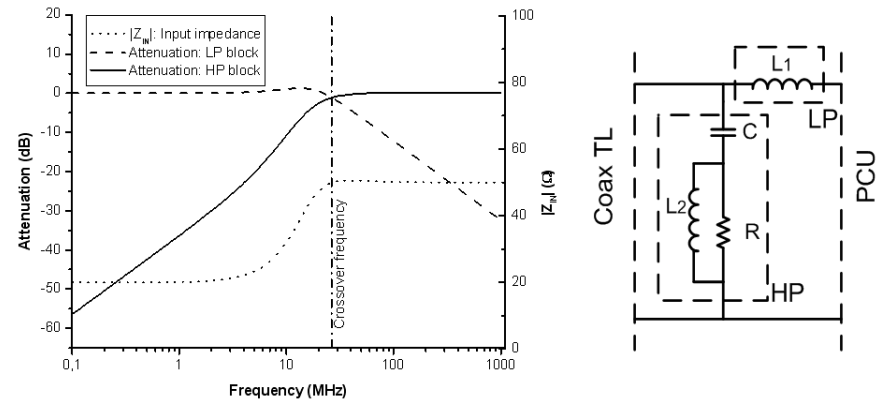

Figure 16. Attenuation properties and impedance of the studied filter (left) and the filter structure (right).

The studied filter was composed of two main blocks, LP and HP. LP is a first order passive low-pass filter. HP is a second order high

pass filter represented by an RLC circuit. The attenuation properties
of the LP and HP blocks are shown in Fig. 16. The main function of
HP was to match the characteristic impedance of the coaxial cable at
high frequencies and to attenuate the induced noise current. LP and
HP formed together a crossover network that should not interfere with
the low-frequency functional signals. Two different realisations of the
filter connected between the cable and the amplifier were compared:

1. Filter realisation 1 including only the LP block.
2. Filter realisation 2 including both the LP and HP blocks.

The current at the PCU end was monitored to evaluate the effectiveness
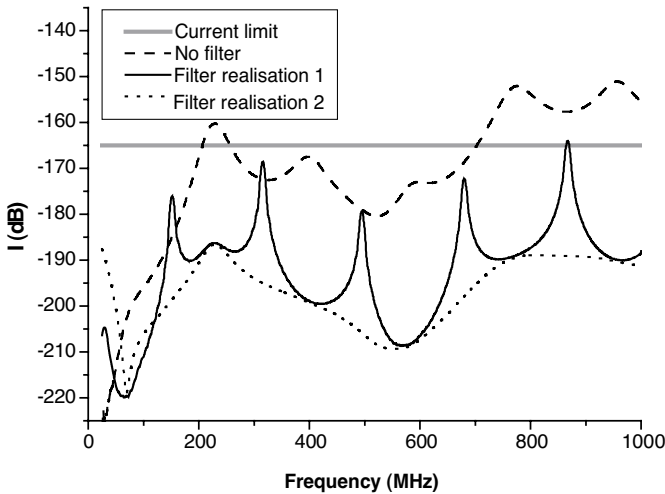of different filter realisations. Results are shown in Fig. 17.

Figure 17.   Current spectrum at the PCU end for different filter
realisations.

Each of the filters inserted at the PCU end reduced the noise
current.   Filter realisation 1 resulted in an average reduction of
the noise current by 20 dB. The current was found to be below the
required maximum level but still showing sharp resonances which could
still jeopardize the functionality of the application. However, when
introducing filter realisation 2 on PCU end, the average reduction of
noise current was 30 dB and the resonances were damped significantly
resulting in a more robust solution for the frequency range of interest.
This could be explained by the fact that impedance matching resistor
reduces reflection and dissipates the high frequency noise current as
expected.   Thus the solution with filter realisation 2 on PCU end

was preferred. The fully assembled wearable system with the double-shielded sensor unit and the matching filter circuit at the amplifier input was tested for EMI immunity, and no false detection alarms of the IR sensor were registered.

5. CONCLUSIONS

The EMC problem was analysed and solved by means of TLM simulations for the wearable system, including sensor unit, connected by 50 cm coaxial cable to a personnel computer unit, all placed along the human skin. The problem originated from immunity tests where false detection alarms of the IR sensor were registered for the frequency range 30 MHz–1 GHz.

The proposed EMC modelling strategy included the procedure of creating a TLM model of the coaxial cable providing controlled EM coupling characteristics. The model was verified with different theoretical EM-coupling models. Furthermore, a comparison to the MoM model was made in order to enhance the confidence in the TLM results. Being a part of the complex wearable system, the circular cross-section coaxial cable was replaced in the model by a square cross-section coaxial cable, which allowed using computationally less expensive grid. Combination of existing transformation methods was found most suitable to ensure the accurate transition to the square cross-section cable model preserving the per-unit-length parameters of the circular cross-section cable.

It is known, that resonance frequencies due to the external cable length cannot be accurately predicted by the solid-block-based TLM model on a coarse grid. Thus, the error can even increase and cause confusion, if EM waves successively propagate in several media as in the case of external field coupling to the coaxial cable. In order to reduce this error in the TLM model, instead of computationally expensive fine mesh it was found efficient to use shorter cable with adjusted dielectric permittivity to preserve the electrical characteristics of the original cable.

Using TLM modelling, it was found that the EM coupling problem consisted in initial coupling of the incident plane wave to the external surface of the coaxial cable shield, and subsequent coupling to the internal circuitry of the wearable system due to imperfect cable shield termination. Analysis of the sensor box designs showed that the shielding effectiveness for a single shield design and the double shield design of the sensor box was on average 20 dB and 30 dB, respectively. The designed filter circuit matching the coaxial transmission line ensured further reduction by 30 dB of the current observed at the

amplifier input, for the frequency range of interest.

Finally, the functional tests showed good performance of the modified wearable system and in this way confirmed the results obtained by the EMC modelling strategy. This demonstrates the efficiency of mathematical modelling in analysing of practical electronics engineering problems.

ACKNOWLEDGMENT

REFERENCES

1. MIL-STD-461E, *Requirements for the Control of Electromagnetic Interference Characteristics of Subsystems and Equipment*, Department of Defense Interface Standards, USA, 1999.
2. Liang, C., X. Shi, and J. Yang, "The variational closed-form formulae for the capacitance of one type of conformal coaxial lines," *Progress In Electromagnetics Research*, PIER 45, 277–289, 2004.
3. White, I., *The VHF/UHF DX Book*, Radio Society of Great Britain, UK, 1995.
4. Tesche, F. M., M. Ianoz, and V. T. Karlsson, *EMC Analysis Methods and Computational Models*, John Wiley & Sons, New York, 1997.
5. Vance, E. F., *Coupling to Shielded Cables*, Wiley-Interscience, New York, 1978.
6. Smith, A. A., *Coupling of External Electromagnetic Fields to Transmission Lines*, John Wiley & Sons, New York, 1977.
7. Swe, T. N. and K. S. Yeo, "An accurate photodiode model for DC and high frequency SPICE circuit simulation," *Nanotech*, Vol. 1, 362–365, 2001.
8. Lo, Y. T., "A note on the cylindrical antenna of noncircular cross section," *J. App. Phys.*, Vol. 24, 1338–1339, 1953.
9. Herring, J. L., *Developments in the Transmission-Line Modelling Method for Electromagnetic Compatibility Studies*, University of Nottingham, UK, 1993.
10. Grant, J. P., R. N. Clarke, G. T. Symm, and N. M. Spyrou, "In vivo dielectric properties of human skin from 50 MHz to 2.0 GHz," *Physics in Medicine and Biology*, Vol. 33, No. 5, 607–612, 1988.